Seismic Performance of Steel Plate Shear Walls Considering Two Different Design Philosophies of Infill Plates. I: Deterioration Model Development

Ronny Purba, Ph.D., A.M.ASCE[1]; and Michel Bruneau, Ph.D., P.Eng, F.ASCE[2]

Abstract: Research was conducted to investigate the seismic performance of steel plate shear walls (SPSWs) having infill plates designed to resist different percentages of the applied lateral loads. The FEMA P695 methodology, which defines the performance in terms of collapse potential under maximum considered earthquake (MCE) ground motions, was used to compare the performance of the SPSWs under consideration. This paper describes the development of component strength deterioration models that are needed to perform the collapse assessment of SPSWs, focusing on stress-strain or force-deformation relationships for infill plates and boundary elements. The approach began with identifying the deterioration and failures modes of SPSW from 36 tested specimens. Cyclic deformation capacities of these SPSWs when reaching their ultimate strength, failure points, and rates of degradation were statistically quantified. Based on these statistical results, initial deterioration models for SPSW components were developed in a format compatible for use with the FEMA P695 procedures. The chosen deteriorated material models for infill plates and boundary elements were calibrated to four selected SPSW specimens varying from one to four stories. A companion paper presents the steps and results of the seismic performance assessments. **DOI: 10.1061/(ASCE)ST.1943-541X.0001098.**

Author keywords: Seismic performance; Steel plate shear walls; Deterioration and failure modes; Deterioration model; Collapse potential; Infill plates design; FEMA P695 methodology; Seismic effects.

Introduction

In seismic design applications, the primary energy dissipating elements of steel plate shear walls (SPSWs) resisting lateral loads are their unstiffened infill plates (webs), which buckle in shear and form a series of diagonal tension field actions (TFAs). From a capacity design perspective, the tension force from the infill plates must be resisted by the surrounding horizontal and vertical boundary elements (HBEs and VBEs). When rigid connections are specified between HBEs and VBEs, and between VBEs and the ground (as specified in many applications of SPSWs), SPSWs also benefit from the moment resisting action of the boundary frame to resist the applied lateral loads. Recognizing the contribution of the boundary frame to the overall strength of the system, Qu and Bruneau (2009) accounted for the attraction that may exist as a means to optimize SPSW designs, rather than relying on the presence of the system overstrength that it may provide to resist the specified lateral loads.

In the current Canadian standard [Canadian Standards Association (CSA) 2009] for the design of steel structures, it is specified that the infill plates of SPSWs must be designed to resist the entire lateral loads, without considering the possible contribution from the surrounding boundary moment resisting frame. Such a statement is not explicitly included in the American seismic provisions (AISC 2010), but one possible interpretation of the AISC design specifications may lead to the same design approach. In this approach, HBEs and VBEs are designed to resist the tension field forces generated by the fully yielded infill plates, and the boundary frame moment resisting action contributing to the global plastic lateral strength of SPSW effectively provides overstrength for resisting the lateral loads. As reported in past experiments, this overstrength in conventional SPSWs can be quite significant. For example, Driver et al. (1997) reported that boundary frame moment resisting action contributed approximately 25% of the global plastic strength of their four-story SPSW specimen. The same observation was made by Berman and Bruneau (2005), who indicated that the boundary frame of their single story SPSW specimen contributed 38% to the total strength of the wall. Qu and Bruneau (2009) demonstrated that the boundary frame moment resisting action can contribute up to 50% of the total strength of an SPSW with an aspect ratio of 2.0 when its boundary elements are designed per capacity design principles. In other words, in such a case, the total lateral strength of the SPSW is twice that needed to resist the total specified lateral loads. This provides a significant incentive to reduce overstrength by explicitly considering boundary frame moment resisting action as contributing to the overall lateral strength of the SPSW.

Qu and Bruneau (2009) investigated this concept of sharing lateral loads between the boundary frame and infill plates, and reported that SPSWs designed per this approach, although having smaller steel quantities, exhibited larger drifts, which suggested that they may need to be designed according to different response modification coefficients (i.e., *R*-factors). They left it to future research to investigate.

This paper, along with a companion paper (Purba and Bruneau 2014b), investigates this matter by quantifying the seismic performance factors (SPFs) for SPSWs having infill plates designed per two different philosophies, to sustain different percentages of the

[1]Instructor, Dept. of Civil Engineering, Univ. of Minnesota, 121 Swenson Civil Engineering, 1405 University Dr., Duluth, MN 55811 (corresponding author). E-mail: rhpurba@d.umn.edu

[2]Professor, Dept. of CSEE, Univ. at Buffalo, 130 Ketter Hall, Buffalo, NY 14260. E-mail: bruneau@buffalo.edu

Note. This manuscript was submitted on September 19, 2013; approved on April 11, 2014; published online on August 5, 2014. Discussion period open until January 5, 2015; separate discussions must be submitted for individual papers. This paper is part of the ***Journal of Structural Engineering***, © ASCE, ISSN 0733-9445/04014160(12)/$25.00.

applied lateral loads. The FEMA P695 methodology (2009b) was selected to accomplish this objective. This methodology provides a rational basis for establishing SPFs for seismic-force resisting systems by assessing the system risks against collapse under maximum considered earthquake (MCE) ground motions.

The validity of the results obtained using this methodology critically depends on the accuracy of the structural numerical models used in these analyses to simulate the component strength deterioration that will eventually lead to global collapse of the system, because these will affect the results of the incremental dynamic analyses used to quantify the SPF [as described in the companion paper (Purba and Bruneau 2014b)]. Although many SPSW specimens in past research have been tested until they exhibited significant strength degradations, and although fragility curves have been developed to relate SPSW damage states to drift values (Baldvins et al. 2012), no attempt to simulate complete strength degradation through numerical investigation was found in the existing literature. Hence, the first key step toward this objective is to develop degradation models for SPSW components (i.e., boundary elements and infill plates).

This paper describes the development of these component strength deterioration models to be used in the collapse assessment of SPSWs, focusing on stress-strain or force-deformation relationships for infill plates and boundary elements. The approach starts with identifying deterioration and failures modes of SPSW observed from 36 tested specimens. Cyclic deformation capacities of these SPSWs when reaching their ultimate strength, failure points, and rates of degradation are statistically quantified. Based on these statistical results, initial deterioration models for SPSW components are developed. The chosen deteriorated material models for infill plates and boundary elements are calibrated to four selected SPSW specimens varying from one to four stories. The development of global structural numerical models and the results of the collapse assessment to determine the corresponding SPFs are presented in the companion paper (Purba and Bruneau 2014b). Beyond the current purpose, the resulting calibrated models can also be valuable to engineers for progressive collapse assessments or performance-based design of individual buildings.

Selecting Degradation Models for SPSW Components

The FEMA 356 document (2000), which was adapted to become the ASCE 41 document (2013), provides provisions for the evaluation and rehabilitation of buildings to improve their seismic performance. In this document, force-displacement capacity of structural components with reliable ductility (prior to exhibiting strength deterioration) are modeled as shown in Fig. 1, commonly known as the backbone curve. Many other backbone models developed in past research on modeling the deterioration of structural components share similarities with the FEMA 356 (2000) backbone model. Two examples can be found in Song and Pincheira (2000) and Ibarra and Krawinkler (2005), which describe models implemented to investigate the cyclic response of nonductile and ductile structures (Song and Pincheira 2000; Haselton and Deierlein 2007; Lignos and Krawinkler 2009).

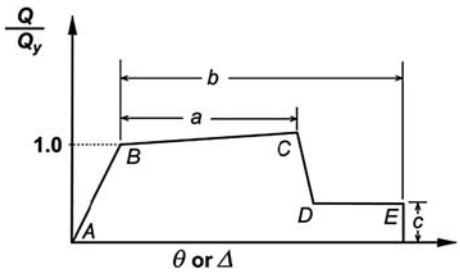

Fig. 1. Force-deformation relations for structural components (courtesy of FEMA 2000)

One of the key differences between those two models and the FEMA 356 (2000) model is that they have less of a sudden degradation slope (i.e., postpeak or postcapping stiffness), which alleviates computational difficulties and the inability to converge in nonlinear dynamic analysis. In addition, they have hysteretic rules to account for cyclic deterioration modes, but this is not the case for the FEMA 356 (2000) model. In other words, structural components modeled according to the FEMA 356 (2000) model only experience strength degradation when cycled beyond Point C, while the component stiffness from one cycle to another cycle of loading remains unchanged. By contrast, structural components modeled according to the last two models may experience stiffness and strength degradation (even before reaching Point C) in addition to strength degradation beyond the capping point. In fact, the Ibarra and Krawinkler (2005) model can simulate strength deterioration in structural components owing to increasing inelastic displacement and repeated cycles of the same displacement, unloading and reloading stiffness degradations, and pinching cyclic strength degradation. It can also simulate structural components that have more severe strength degradation under cyclic loading than under monotonic loading (i.e., the cyclic envelope is smaller than the force-displacement backbone boundary).

Beyond backbone-type models, there exist many sophisticated hysteretic models that are able to incorporate stiffness degradation, strength degradation, or a combination of both deteriorations. An extensive review of these hysteretic models can be found elsewhere (FEMA 2009a). The question remains as to which models are appropriate to model SPSW components up to failure, and whether cyclic degradation rules should be considered. Observations of force-displacement hysteretic curves for SPSW specimens in past experimental research provides guidance about how to select appropriate deterioration models for SPSW components (several examples are presented in later sections). Relating those to the hysteretic rules for cyclic deterioration, several observations can be made, as follows:

1. Up to the capping point (i.e., defined as the point of maximum strength before strength degradation starts to occur), stiffness both during loading and unloading are slightly similar between hysteretic loops. Moderate changes in stiffness are only observed after strength degradation occurs. This behavior indicates that incorporating stiffness degradation in the deterioration models for SPSW components is not crucial for the type of collapse analysis of SPSWs intended in this research.
2. Strength degradation owing to repeated cycles at the same displacement is relatively small; as such, it can be neglected in developing deterioration models for the SPSW components.
3. Strength degradation primarily occurs when the increasing inelastic displacements pass the capping point in the backbone curve. Therefore, the cyclic envelope can be designated as similar to the force-displacement backbone boundary.
4. The significant pinching behavior exhibited in the hysteretic curve of these SPSWs is a consequence of the fact that the unstiffened infill plates behave analogously to slender, tension-only bracing. That behavior can be captured directly when modeling the wall with tension-only nonlinear braces. Detailed information on the behavior of unstiffened infill plates can be found elsewhere (Roberts and Sabouri-Ghomi 1991; Berman and Bruneau 2005).

Hence, the simple force-displacement backbone curve without cyclic degradation rules is sufficient to represent degradation models for boundary elements and infill plates in SPSWs. Here, degradation parameters, such as plastic deformation when reaching the capping point and postcapping stiffness (i.e., rate of degradation) will be estimated in a probabilistic framework (Ibarra and Krawinkler 2005), determined based on the results of previous SPSW experiments. Quantification of these degradation parameters for both infill plates and boundary elements, and whether or not residual strength should be considered, is addressed in this paper.

Identification of Deterioration and Failure Modes

To quantify the degradation parameters for SPSW components, a detailed literature review of SPSW experimental results from research in the past 30 years was conducted. This review was intended to investigate three specific objectives: (1) to identify the deterioration modes associated with the loss of strength and failure modes that occurred at the end of each test; (2) to statistically quantify at which story drift the capping and failure points occurred; and (3) to statistically quantify the rate of degradation, which is defined as the ratio between strength drop and drift range from the failure to the capping points. A total of 36 conventional unstiffened slender-web SPSW specimens were examined for which testing data were adequately reported and accessible at the time of this writing. The specimens varied from single-story to four-story SPSWs with aspect ratios ranging from 0.7 to 2.2. Both welded and bolted connections were used in these walls, either connecting infill plates by means of fish plates to boundary frames or connecting horizontal to vertical boundary elements.

Inferred from the experimental data considered here, the possible causes of deterioration of structural components that lead to failures of SPSWs consist of deteriorations associated with web tearing, flexural or shear failure of boundary elements, and instability of boundary elements. Each deterioration mode is described in detail in the following.

Web Tearing

Past experiments have shown that relatively small fractures of infill plates have insignificant degrading impact on the structure's ultimate strength, (Lubell et al. 2000; Astaneh-Asl and Zhao 2002; Vian and Bruneau 2005; Li et al. 2010). Because infill plates provide superior redundancy to transfer tension forces to surrounding boundary elements, cracks in one part of a plate strip may only locally disturb the regularity of the tension stress flows. As such, stresses can flow around and redistribute tension stresses to adjacent uncracked parts of the infill, maintaining TFA throughout the loading history.

Web tearing (WT) contributes to the deterioration of SPSW strength only if fractures of infill plates propagate to significant lengths, which can render parts of the infill plates unable to develop TFA. As a result, infill plates progressively lose their capacity to sustain loads. Examples of this deterioration mode can be found in specimens tested by Qu and Bruneau (2008) and Choi and Park (2009). In the first example, the cracks initially occurred at the corner of the panel, then propagated to the connections of infill plates with vertical and horizontal fish plates; in the second example, the cracks also initially occurred at the same location, but this time propagated to the middle part of the infill plates.

Failure of Boundary Elements

Failure of boundary elements (FBE) can be classified as either flexural failure, shear failure, or member instability. Flexural failure observed in past experiments can be classified into the following types of damage: (1) plastic hinge development at boundary element ends with ductile strength degradation owing to localized flange or web buckling; (2) weld fracture at the connections between HBEs and VBEs or between VBEs and their base; (3) fracture of the boundary elements away from the connections [i.e., at the center line of plastic hinge, particularly in HBEs with reduced beam section (RBS) connections where fractures have occurred near the midlength of the reduced flange segment]; and (4) shear tab failure that leads to HBE web and flange fractures.

Shear failure is characterized by shear yielding of a significant length across the web of VBEs, which causes lower expected VBE plastic moments and can result in significant VBE inward deformations (i.e., hourglass shape deformations) owing to the pulling forces from yielded infill plates. Several examples of flexural and shear failures can be found in past studies (Driver et al. 1997; Lubell et al. 2000; Vian and Bruneau 2005; Park et al. 2007; Qu and Bruneau 2008).

Deterioration mode associated with instability of boundary elements (IBE) has been occasionally reported in past experiments. Global instability was reported to associate with out-of-plane (weak-axis) buckling of VBEs or lateral-torsional buckling of HBEs; this occurred in the early stages of loading (i.e., as early as 1% drift). Examples of IBE deterioration mode can be found in past studies (Caccese et al. 1993; Elgaaly 1998; Lubell et al. 2000).

Shear failure and IBE are unlikely to occur in a well-designed SPSW because they can be prevented by designing boundary elements according to capacity design principles and by selecting seismically compact sections to prevent local and global buckling. Therefore, these failure modes are ruled out as limit states to be considered in applying the FEMA P695 methodology (2009b); only the two ultimate failure modes of well-designed SPSWs, WT and FBE, are considered in this research for quantifying the deterioration parameters in SPSW. The results are presented in the following section.

Statistical Estimation of Cyclic Deformation Capacity

Among the 36 SPSW specimens under examination, a large variability of experimental outcomes was observed. To avoid a biased statistical interpretation of cyclic deformation capacity at the ultimate (capping) and failure points, only the specimens that were pushed beyond the ultimate point and exhibited stable deterioration with gradual strength drop were considered, as listed in Table 1 for 17 selected specimens. A complete list of SPSW specimens can be found in (Purba and Bruneau 2014a). On average, SPSW specimens reached their ultimate strength at 3.1% drift.

Regarding the condition at the failure point, cyclic deformation capacity and percentage of strength degradation need to be estimated. The average SPSW cyclic capacity when reaching the failure point (when substantial WT, FBE, or a combination of both deterioration modes occurred and the tests ended) was 4.5% drift. When reaching the failure points, SPSW specimens lost approximately 25% of their ultimate strengths. Many tests were stopped after a substantial drop in strength was observed (25%, on average), and the actual rate of progression of further damage that would have occurred beyond that point is not known for those specimens.

Table 1. Steel Plate Shear Walls of Tested Specimens

Researcher	Specimen	Number of stories	Geometric properties			Type of connection[a]		Condition at ultimate			Condition at end			
			L_p (mm)	H_s (mm)	Aspect ratio	Frame	Infill	Mode	V_{max} (kN)	Drift (%)	Mode	V_{end} (kN)	Drift (%)	μ^g
Driver et al. (1997)	—[b]	4	3,050	1,776	1.7	W	W	WT	3,080	2.2[c]	FBE	2,618	4.0[c]	9.0
Lubell et al. (2000)	SPSW2	1	900	900	1.0	W	W	FBE	250	4.00	FBE	175	5.0	7.5
Astaneh-Asl and Zhao (2002)	UCB-1	2	—[b]	3,100	—[b]	W	W	FBE	4,005	3.3[c]	FBE	2,403	4.0[c]	5.7
	UCB-2	3	—[b]	2,067	—[b]	W	W	FBE	5,451	2.2[c]	FBE	4,066	3.0[c]	4.3
Behbahanifard et al. (2003)	—[b]	3	3,050	1,678	1.8	W	W	FBE	3,500	2.6[c]	WT	2,850	3.7[c]	7.9
Berman and Bruneau (2005)	F2	1	3,658	1,829	2.0	P	W	WT	620	3.0	WT	420	3.7	12
Vian and Bruneau (2005)	P	1	4,000	2,000	2.0	W+RBS	W	FBE	1,790	2.0	FBE	1,650	3.0	10
	CR	1	4,000	2,000	2.0	W+RBS	W	FBE	2,050	2.5	FBE	1,340	4.0	13.3
Park et al. (2007)	SC2T	3	1,750	1,100	1.6	W	W	FBE	1,663	2.6[d]	FBE	1,338	3.8[e]	7.0
Qu et al. (2008)	—[b]	2	4,000	4,000	1.0	W+RBS	W	FBE	4,245	3.3[c,f]	WT	2,387	5.2[c,f]	10.4
Choi and Park (2008)	FSPW1	3	1,650	1,075	1.5	W	W	FBE	1,392	3.6[d]	FBE	1,364	5.2[e]	8.1
	FSPW2	3	2,350	1,075	2.2	W	W	FBE	1,817	4.5[d]	WT	1,776	5.6[e]	11.8
	FSPW3	3	2,350	1,075	2.2	W	W	FBE	1,565	2.7[d]	FBE	1,100	5.4[e]	10.6
Choi and Park (2009)	BSPW1	3	2,350	1,075	2.2	W	P	WT	1,882	3.6[d]	WT	1,200	5.3[d]	11.8
	BSPW2	3	2,350	1,075	2.2	W	P	WT	1,961	3.3[d]	FBE	1,05d5	5.3[d]	11.0
Li et al. (2010)	N	2	2,140	3,250	0.7	W+RBS	W	FBE	1,300	4.0[e]	FBE	1,105	5.0[e]	12.5
	S	2	2,140	3,250	0.7	W+RBS	W	FBE	1,070	3.0[e]	WT	910	5.3[e]	12.5

[a]P = pin (simple) or partial welded connection; W = welded (rigid) connection; RBS = reduced beam section.
[b]Not available.
[c]First story drift.
[d]Top story drift.
[e]Maximum interstory drift.
[f]Information from Phase II (i.e., cyclic test).
[g]$\mu = \Delta_{end}/\Delta_{yield}$.

In the preceding approach, both cyclic deformation capacity and percentage of strength degradation at the failure point were treated as independent statistic variables. Another approach in which both parameters were treated as two related statistical variables was investigated. The process started by preparing a backbone curve of the cyclic hysteresis for each specimen from the ultimate to the failure points. For a certain percentage of strength degradation beyond the capping point, the corresponding story drift at this degradation level was recorded for each specimen; then, for all specimens, average and SD values were calculated. Interestingly, this slightly more elaborate approach produced results only marginally different from those obtained by using the first approach (i.e., 25% strength degradation at approximately 4% drift).

Several other factors may affect cyclic deformation capacities of specimens when reaching the capping and failure points, such as panel aspect ratio, specimen scales that dictate boundary element sizes, boundary element compactness, and types of connections between SPSW components and between specimens and their bases. In addition to these factors related to specimen geometric properties, the design approaches used to size the SPSWs (e.g., elastic design, plastic design, or capacity design principles designing specimens as shear-type structures, flexural-type structures, or a combination of both) and loading protocol imposed during experiments (e.g., level of axial loads imposed, distribution of lateral loads along the specimen height for multistory specimens) may affect specimen capacities to resist earthquake loads. However, in light of the relatively small number of SPSW specimens tested at the time of this writing, the effect of these factors on specimen cyclic deformation capacities cannot be statistically investigated and is considered to be beyond the context of this research. As new data become available, the effect of these factors and relationships between these factors may be quantified.

Initial Deterioration Models for SPSW Components

The preceding cyclic deformation capacities for the capping and failure points were capacities at the structural level. To model deterioration for SPSWs using structural analysis software, similar information needs to be developed at the component level. In other words, assuming that the degradation pattern at the structural level is an expression of behavior at the component level, moment-rotation and axial force-deformation degradation models are required for boundary elements and infill plates, respectively. These models are usually developed from past component tests or past assembly of structural system tests that reported these local behaviors. However, because neither of these sources is available for SPSWs at the time of this writing (in a way that would uncouple infill and boundary element contributions), initial deterioration models were developed for boundary elements and infill plates indirectly from the available structural-level responses.

This can be achieved by first developing numerical models of several selected specimens, performing monotonic pushover analysis, and recording local behaviors when the structure experienced 3 and 4% interstory drift (i.e., corresponding to the capping and global failure points). In the analysis of strip models, both steels used for boundary elements and infill plates were represented by an idealized elasto-perfectly plastic stress-strain material. To consider strength degradation, yield strengths of both steels used for boundary elements and infill plates were afterward assigned a 25% strength drop at the failure point based on the statistical results presented in the previous section. For this purpose, the specimens selected were those of Vian and Bruneau (2005), Qu and Bruneau (2008), Choi and Park (2009), and Driver et al. (1997). Detailed information and the rationale for selecting these single-story to four-story specimens are addressed in the next section. The resulting initial degradation models are shown in Fig. 2 for boundary elements and infill plates. The degradation parameter

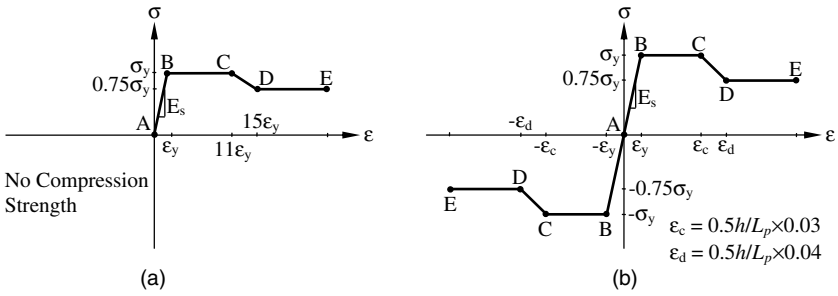

Fig. 2. Initial degradation models: (a) strips; (b) boundary elements

values shown in the figure represented the average values of four specimen local behaviors at 3 and 4% drifts.

Although both deterioration modes (i.e., WT and FBE) generally take place once SPSW specimens are cycled to relatively large lateral displacements (or drifts), many past experiments reported that infill plates can continue to dissipate energy even after failure of boundary elements. In such cases, infill plates exhibited nondeteriorating WT with significant inelastic deformations. Hence, it may be tempting to consider modeling deteriorating SPSWs by implementing strength deterioration models only for the boundary elements while providing elasto-perfectly plastic model without deterioration for infill plates. The problem with this approach is that when significant WT occurs, as observed in several other tests, it may provide incorrect results.

Another legitimate question is whether the residual strength defined for infill plates in Fig. 2(a) is appropriate, considering that once significant tears start to propagate across the infill, the corresponding strip plate used in the model at this location should lose its entire strength to sustain loads (i.e., the stress it carries should completely drop to zero when tears start to propagate). Furthermore, given that WT that is correlated to strength degradation generally starts from one of the panel corners, an accurate model should presumably account for the fact that strips attached closer to the panel corner lose strength faster than the others. The impact is unclear of using different deterioration models for strips, depending on their location from the panel corner.

To investigate these concerns, a series of monotonic pushover analyses was conducted with various deterioration models assigned to boundary elements and infill plates. More specifically, these analytical investigations were intended to compare the global SPSW deterioration behavior when deterioration models were assigned to both infill plates and boundary elements for the case in which a deterioration model was only assigned to either boundary elements or the infill plates. In addition, impact of severe and moderate deterioration models assigned to corner and middle strips, respectively, was investigated and compared with the case of uniform deterioration models. Finally, different deterioration rates for infill plates were investigated, considering abrupt drop to zero stress at a certain specified strain level and gradual drop to zero stress at various rates. Based on the findings of this parametric study, reported comprehensively in Purba and Bruneau (2014a), the initial degradation models were modified by calibrating proposed degradation models to available experimental data. By matching the results of analyses using these numerical models to their corresponding experimental results, key deterioration model parameters (i.e., the capping Point C and the residual strength Point D in Fig. 2) for boundary elements and infill plates could be estimated.

Calibration of Proposed Deterioration Model

Calibration of the proposed deterioration models was conducted by using four selected specimens that represent single-story to four-story SPSWs with panel aspect ratios ranging from 1.0 to 2.2. Each specimen has a unique characteristic for which observation of different scenarios of strength degradation can be made. The single-story specimen examined by Vian and Bruneau (2005) exhibited fractures of boundary elements but no fractures of its infill plates that contributed to the specimen strength degradation (i.e., the infill plates exhibited significant plastic deformations instead). The reverse scenario was observed in the three-story specimen tested by Choi and Park (2009), in which strength deterioration was attributed to WT in the absence of significant damages to boundary elements. A case in which both fracture of boundary elements and deterioration owing to WT was reported by Qu and Bruneau (2008) for a two-story specimen. Although both deterioration modes were also observed in the four-story specimen of Driver et al. (1997), the strength degradation rate and magnitude of this degradation were not as severe as in the two-story specimen. Considering that the four calibrated specimens already covered the ranges of aspect ratio, number of stories, drift capacities at the ultimate and end conditions, and amount of strength degradation for the specimens reported in Table 1, additional calibration was not conducted and the four calibrated specimens were deemed adequate to represent the intended calibration results.

Based on documented experimental information reported for each specimen (e.g., geometric and section properties, material properties, presence of gravity loads, lateral load distributions, and cyclic pushover displacement loading histories), a strip model was developed in *OpenSees* for each specimen. The strip model consists of series of tension strips, typically of equal width, pin-connected to the surrounding boundary elements, and inclined in the direction of the tension field, α, estimated per Eq. (F5-2) of AISC (2010) that considers geometric properties of the infill plates and boundary elements at the story level of interest. A minimum of 10 strips per panel is required to accurately represent the infill plate behavior (Thorburn et al. 1983) and the width of each strip (S_{diag}) can be calculated as ($L \cos\alpha + H \sin\alpha$) divided by the number of specified strips, where L and H are the width and height of the panel. In the case of multistory SPSWs, equally spaced strips with slightly different tension field angles from one story level to another most likely result in a strip model having staggered node points at the HBE in adjacent stories. However, for practical purposes, it is preferable to use a strip model in which the strips have the same inclination angle at all stories (i.e., using the average of the tension field angle of all panels) and have common nodes at the HBE in adjacent stories. Such slight variations in angle have insignificant consequences on the results (Dastfan and Driver 2008). Furthermore, an eccentricity exists between boundary element

centerlines and the edge of the infill plate; this rigid offset was not included, but instead, strips were directly connected the boundary elements. This simplification is reasonable in the current context and is of negligible impact on the results of this particular study. The validity of the strip model to accurately represent the nonlinear behavior of SPSWs is well established (Driver et al. 1997; Elgaaly 1998; Berman and Bruneau 2005; Qu and Bruneau 2008).

Moreover, unstiffened infill plates were modeled as series of truss elements in *OpenSees* oriented in the direction of the tension field. The hysteretic uniaxial material model was selected to define the inelastic behavior of these truss elements. Boundary elements were modeled by using the beam with concentrated hinge (BCH) element with fiber sections and hysteresis uniaxial material model. The concentrated hinge with fiber sections automatically accounts for the interaction between the axial loads and moments that can occur in the boundary elements. Although it was not considered in this research, the axial force entering SPSW in different proportions from the respective adjacent bays would have been automatically accounted for, but variations on the percentages coming from the left and right sides (by drag forces from adjacent bays) were not considered in this study. Their impacts on the seismic performance of SPSWs, however, are considered beyond the scope of this research. Detailed information and the rationale for selecting these elements can be found in Purba and Bruneau (2014a).

Before performing cyclic pushover analysis to simulate the actual experimental program, a series of monotonic pushover analyses was conducted to determine a monotonic pushover force-displacement curve that matched the backbone of the force-displacement hysteretic curve obtained in the experiment. A strain hardening of 2% up to the capping point and an assumed zero-slope plateau of no strain hardening beyond this point was assigned to the stress-strain material properties of the axial hinges and to each fiber in boundary element plastic hinge model. Although strain hardening would likely be more substantial in boundary elements than in infill plates, for simplicity, strain hardening was assigned to be identical for the steels used for the boundary elements and strips. Once a good match between the resulting monotonic pushover curve and the backbone of hysteretic curve from the experiment was obtained (i.e., matching the key deterioration parameters at Points C and D), cyclic pushover analysis was conducted following the actual displacement loading histories imposed during each experiment. In this calibration process, only one cycle of loading history was applied at each displacement increment level, because no in-cycle material degradation was included in the numerical model.

Several iterations were typically required to achieve a good match between the numerical and experimental results, which included revising parameters at Points C and D defined for both boundary elements and strips, slightly increasing yield strength of steels used for boundary elements and strips by a factor of 5–10%, and reanalyzing the strip model under monotonic and cyclic pushover analysis. The slight increase of material strength above the reported value was deemed necessary to obtain a better match between the numerical and experimental results. This increase is within the range of material property variability obtained from the coupon test, and was therefore deemed acceptable.

Additionally, for the four calibrations presented in the subsections that follow, specimen dimensions, material properties, and details of the experimental program can be found in the original work by the researchers and are not repeated here owing to space constraints. Failure modes, strength degradation, and corresponding deformation capacities are reported here as a basis for defining deterioration models of SPSW components.

Single Story SPSW: Vian and Bruneau Specimen

The first calibration was conducted on the single-story SPSW specimen tested by Vian and Bruneau (2005). Bottom flange fractures at both RBS locations of the lower HBE occurred at 3.0% interstory drift and caused a strength degradation of 17.5% from the specimen ultimate strength of 2,060 kN, which was reached in the previous displacement cycle of 2.5% interstory drift. Moreover, fractures at the connection of the upper HBE to the VBE occurred at 4.0% interstory drift and caused a strength degradation of 24% from the ultimate strength of the specimen. Regarding the infill plate, noticeable plastic deformations and minor cracks were observed but had insignificant impacts on the overall deterioration behavior of the specimen. In the strip model developed for this specimen (Fig. 3), a deteriorating material model was assigned to the HBEs and an elasto-plastic material model was assigned to the infill plates. Although they are not shown in Fig. 3(a) for clarity, strips were actually added in the opposite directions at the same inclination angles to those shown in the figure to account for reorientation of the tension field direction as the loading excursion changes.

The resulting force-displacement hysteresis of the strip model is shown in Fig. 3(d), plotted with that of the cyclic pushover test. Overall, the analytical hysteresis agrees well with that from the experiment. The hysteresis more accurately matches the capping point and the degradation backbone up to the completion of the test in the positive excursion compared to that in the negative excursion. Moreover, the strip model exhibited more severe pinching behavior than that observed during the experiment. This discrepancy is attributed to the material model assigned to the infill plate that can only yield in tension and has no strength in compression, which will be further addressed in a later section.

Two-Story SPSW: Qu and Bruneau Specimen

Qu and Bruneau (2008) conducted an experimental program on a full-scale, two-story steel plate shear wall with RBS connections and composite floors. When reaching the capping point at 3.0% first story drift, the maximum base shear recorded was 4,245 kN. At the conclusion of the experiment after the specimen was cycled up to a maximum first story drift of 5.2%, the base shear strength dropped approximately 44% from its ultimate strength as a result of significant WT in the first story infill plate and fracture of the intermediate HBE. Interestingly, except for insignificant tearing at the corners of the second story infill plate, no major fractures were reported in either the infill plate or boundary elements of the upper story and no strength deterioration occurred in that story. Hence, in the strip model developed for this specimen, deteriorating material models were only assigned to most of the first story strips and intermediate HBE, whereas elasto-plastic material model with 2% strain hardening up to the capping point was assigned to the remaining members. Inferred from the experimental step-by-step observations reported in Qu and Bruneau (2008), fracture of the intermediate HBE occurred at the onset of the 3.0% first story drift and strength degradation stabilized at 3.7% first story drift. In addition, WT in the first story infill plate started at the upper north corner when the specimen experienced 3.0% first story drift and progressed toward the upper south corner and the bottom north corner at 4.8% first story drift. At the conclusion of the test, the first story infill plate was practically torn away from the intermediate HBE. Hence, in the numerical model (Fig. 4), strips losing their capacity to sustain lateral loads were modeled in sequence according to the fracture propagation.

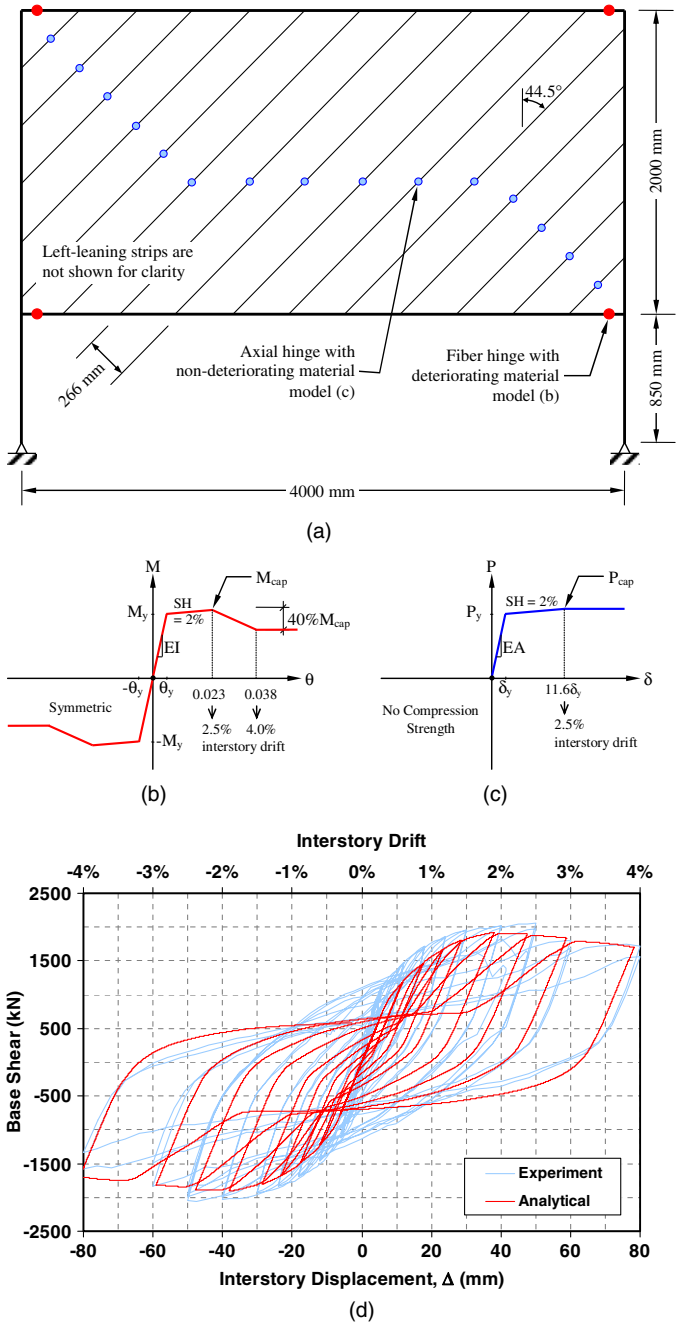

Fig. 3. Calibration of the single story SPSW specimen tested by Vian and Bruneau (2005): (a) strip model; (b) material model for boundary elements; (c) material model for strips; (d) resulting hysteresis curve

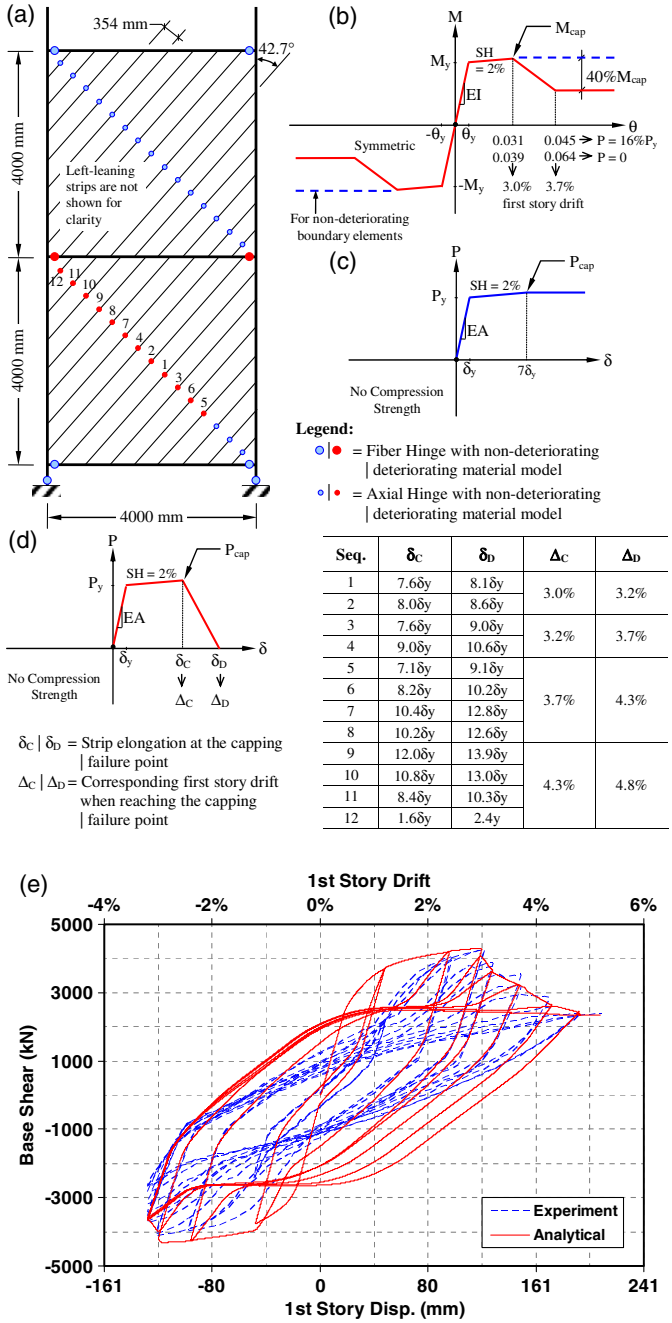

Seq.	δ_C	δ_D	Δ_C	Δ_D
1	7.6δy	8.1δy	3.0%	3.2%
2	8.0δy	8.6δy		
3	7.6δy	9.0δy	3.2%	3.7%
4	9.0δy	10.6δy		
5	7.1δy	9.1δy	3.7%	4.3%
6	8.2δy	10.2δy		
7	10.4δy	12.8δy		
8	10.2δy	12.6δy		
9	12.0δy	13.9δy	4.3%	4.8%
10	10.8δy	13.0δy		
11	8.4δy	10.3δy		
12	1.6δy	2.4y		

Fig. 4. Calibration of the two-story SPSW specimen tested by Qu and Bruneau (2008): (a) strip model; (b) material model for boundary elements; (c) material model for nondeteriorating strips; (d) material model for deteriorating strips; (e) resulting hysteresis curve

The resulting force-displacement hysteresis of the strip model is shown in Fig. 4(e), plotted with that from the cyclic pushover test. Overall, the analytical hysteresis agrees well with that from the experiment. It matches the capping point and the degradation backbone up to completion of the test. Although the analytical hysteresis is noticeably larger than that recorded in the experiment in the early stages of the hysteretic behavior, this discrepancy is attributable to the inelastic excursions recorded during the pseudo-dynamic test before the cyclic pushover test, which were not accounted for in the numerical analysis (i.e., the infill plate contribution to strength of the SPSW up to the drift reached during the pseudo-dynamic tests could not be mobilized until drift exceeded these drifts in the cyclic tests).

Three-Story SPSW: Choi and Park Specimen

One of the three-story SPSW specimens of Choi and Park (2009) (i.e., denoted as BSPW2) was selected for this calibration process. When reaching the capping point at 3.3% top story drift in the positive excursion, the maximum base shear was 1,961 kN. Although the initiation of WT was observed in the first and second story infill plates prior to reaching the capping point, it did not affect the overall capacity of the structure to sustain lateral loads. The base shear strength significantly dropped to 1,524 kN in the subsequent displacement step of 4.4% top story drift when major plate tearing occurred in the second story infill plate. At completion of the test, WT had propagated to almost the entire area of the second story

infill plate, causing the base shear strength to drop by approximately 46%, to 1,055 kN at 5.3% top story drift. Based on this failure mechanism, in the strip model developed for this specimen (Fig. 5), deteriorating material models were assigned to most of the strips at the second story. Minor plate tearing and plate kinking in the first and third story infill plates were considered to be nondeteriorating web tearing (NWT); therefore, an elasto-plastic material model with 2% strain hardening up to the capping point was used at these stories instead of a deteriorating material model. Moreover, flange fracture at the upper end of the second story VBE occurred in the last cycle of displacement loading. However, because no indication reported that this fracture initiated at an earlier cycle of displacement loading, all boundary elements were considered to have nondeteriorated material model similar to the strips at the first and third stories.

As in the calibration process for the Qu and Bruneau (2008) specimen, strips at the second story of the Choi and Park (2009) specimen lost their capacity to sustain lateral loads sequentially.

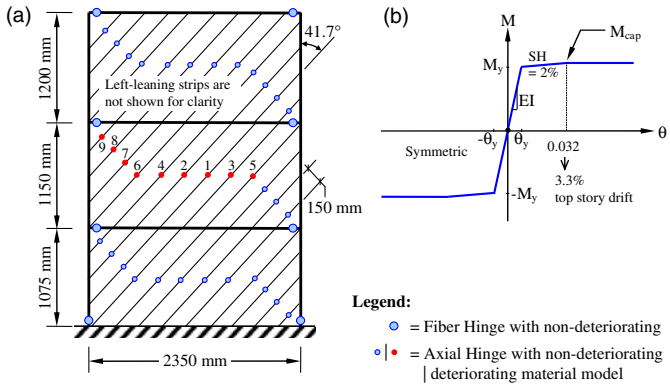

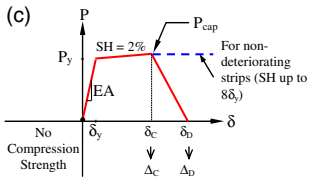

δ_C | δ_D = Strip elongation at the capping | failure point

Δ_C | Δ_D = Corresponding top story drift when reaching the capping | failure point

Seq.	δ_C	δ_D	Δ_C	Δ_D
1	11.9δy	14.9δy	3.3%	3.7%
2	11.9δy	14.9δy		
3	11.7δy	14.9δy		
4	11.7δy	14.9δy		
5	17.8δy	19.6δy	4.4%	4.8%
6	17.7δy	22.8δy		
7	14.4δy	25.8δy	4.6%	5.3%
8	16.7δy	25.3δy		
9	17.0δy	27.5δy		

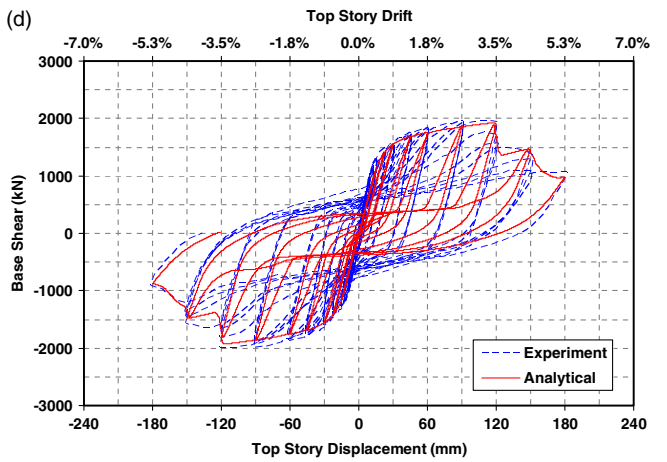

Fig. 5. Calibration of the three-story SPSW specimen tested by Choi and Park (2009): (a) strip model; (b) material model for boundary elements; (c) material model strips; (d) resulting hysteresis curve

This started from middle strips at the onset of 3.3% top story drift and gradually propagated toward strips adjacent to the upper left and lower right corners at 5.3% top story drift. The resulting force-displacement hysteresis of the specimen model is shown in Fig. 5(d), plotted with that from the cyclic pushover test. Overall, the two hysteresis values agree well with negligible discrepancies at the onset of effective yielding, the capping point, and the degradation backbone up to completion of the test. However, the two hysteresis values exhibit slightly different pinching behavior. Similar to the calibration results for the Vian and Bruneau (2005) case, the strip model exhibited severe pinching behavior, as opposed to the moderate pinching behavior observed during the experiment.

Four-Story SPSW: Driver et al. Specimen

The specimen tested by Driver et al. (1997) is the only four-story SPSW specimen (at the time of this writing) tested up to its ultimate capacity and that exhibited stable hysteretic behavior and strength degradation behavior. The maximum base shear of 3,080 kN was reached at 2.2% first story drift ($= 5\delta_y$). Minor WT at the top west corner of the first story infill plate and flange local buckling at both ends of the east VBE1 (i.e., below HBE1 and near the base) and at the upper end of the west VBE1 were reported in earlier cycles before reaching the capping point. As the WT propagated to a larger size and the severity of VBE flange local buckling increased, the lateral strength of the specimen started to deteriorate. However, the degradation rate was relatively slow compared to that of the other three specimens under consideration. In this case, the specimen base shear strength only dropped 15% from the maximum base shear at the end of the 4.0% first story drift cycle ($= 9\delta_y$). Structural damage predominantly concentrated at the first story level as a result of the selected uniform loading distribution.

In the strip model developed for this specimen (Fig. 6), deteriorated material models were only assigned to VBE1 and several strips in the first story infill plate, whereas an elasto-plastic material model with 2% strain hardening up to the capping point was assigned to the remaining members. It was considered that the aforementioned minor WT and VBE flange local buckling prior to the capping point insignificantly impact the overall strength of the specimen. As such, strength degradation in the strip model was set to start at 2.2% first story drift.

The resulting force-displacement hysteresis of the strip model is shown in Fig. 6(d), plotted with that from the cyclic pushover test. As with the other three calibration results, the resulting analytical hysteresis of the four-story specimen agrees well with that from the experiment, which matches the capping point and the degradation backbone up to the completion of the test. However, as a consequence of excluding in-cycle strength degradation in the material model, numerical strength degradation remained at the same level after $5.4\delta_y$ excursion in the negative direction. Again, the strip model exhibited more severe pinching behavior than that observed during the experiment, which is attributed to the fact that the material model assigned to the infill plates can only yield in tension and has no compression strength.

Interpretation of Calibration Results

In general, the numerical model underestimated the onset of effective yielding observed in the experiment. No substantial effort was invested to resolve this discrepancy in the calibration process because underestimating the onset of effective yielding was considered to not critically affect the collapse prediction of SPSWs.

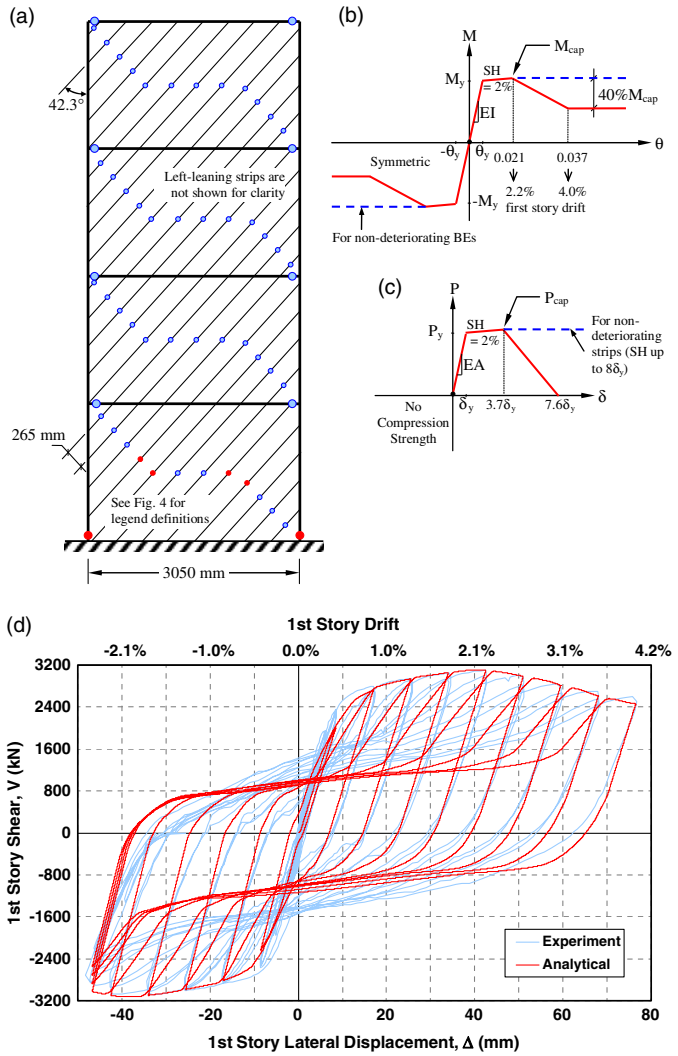

Fig. 6. Calibration of the four-story SPSW specimen tested by Driver et al. (1997): (a) strip model; (b) material model for boundary elements; (c) material model strips; (d) resulting hysteresis curve

Although, in all cases, the calibration process successfully matched the capping point and the backbone of the degrading hysteresis, discrepancies in pinching behavior were observed between the numerical and experimental results. One possible explanation for this underestimation of the experimental pinching behavior is that the strip material models exclude the compressive strength that can develop during loading reversal. This assumption is reasonably correct to simulate infill plate behavior in earlier cycles. However, it has been observed in some cyclic tests that after SPSWs undergo substantial inelastic elongation, the infill plates can exhibit significant compressive strength during load reversal, as reported by Clayton et al. (2012). When including compressive strength during reversal of loading in the material model for the infill plates, Choi and Park (2010) successfully simulated the pinching behavior observed in the Driver et al. (1997) experiment. However, their numerical model failed to simulate the deteriorating hysteresis behavior after the capping point. During the calibration process, no effort was made to resolve the underestimated pinching behavior because it was considered to have a marginal impact on the overall collapse performance of steel plate shear walls. Furthermore, recent tests by Dowden and Bruneau (2014) showed that the effect of this compressive strength was insignificant in shake table tests (as opposed to cycling testing). Hence, the compressive strength of the strip was excluded from the final strip deterioration model.

Behavior of Selected SPSW Specimens and Final Deterioration Models for SPSW Components

Considering the preceding calibration results, particularly the fact that different models were used to replicate each of the four experimental results, one might ask which of these degradation parameters should be selected to generally capture the degradation of boundary elements and infill plates in any specific SPSW. Because only a limited number of specimens was calibrated, the approach selected here was to examine the worst degradation parameters from the preceding cases, as opposed to the average values of all four specimens. Hence, for the collapse assessment of steel plate shear walls, degradation models for boundary elements and infill plates were selected from the calibration results of the two-story SPSW specimen of Qu and Bruneau (2008). The model for boundary elements in Fig. 4(b) was calibrated for the condition when HBE1 experienced axial loads, P, equal to 2,193 kN (i.e., P = 16% Py). To apply the model to other specimens, the model was first modified for the condition at zero axial loads. The updated rotation capacities for the capping point and the point corresponding to 40% degradation of moment capacity for boundary element model are 0.039 and 0.064 rad, respectively [Fig. 4(b)]. Regarding the infill plates, the strip model was based on results of deterioration of the first strip. As shown in Fig. 4(d), the strip deformation capacities at the capping and failure points were $7.6\delta_y$ and $8.1\delta_y$, respectively (corresponding to 1.3 and 1.4% axial strain, respectively).

To examine the impact of selecting the most conservative deterioration models (i.e., the models with the most severe degradation), another set of analyses was conducted on all calibrated specimens. The resulting hysteresis values for all calibrated specimens using the conservative deterioration models are shown in Fig. 7. As expected, because the conservative deterioration models were selected from the Qu and Bruneau (2008) specimen, the analytical result was close to the calibration result of the experimental hysteresis in that case. In the specimen of Vian and Bruneau (2005), the conservative model actually delayed degradation, which had moved from 2% interstory drift in the experiment to 3.3% interstory drift in the analysis. However, beyond this point, strength degradation was significant and abrupt. In other words, deterioration of infill plates and boundary elements occurred at similar times. Significant differences were observed in the Choi and Park (2009) specimen. Strength degradation started to occur at 2.7% drift, which is sooner than in the actual experiment, where it happened at 3.5% drift. In addition to boundary element deterioration, all strips lost strength by 3.5% drift and only the second story infill plate lost strength at 5.3% drift in the actual experiment. Finally, for the Driver et al. (1997) specimen, a similar response to that reported in the actual experiment was observed in this specimen, up to 2.1% top story drift. Beyond this point, however, faster strength degradation was observed in the conservative case within the positive excursions, but not for the negative excursions. At the conclusion of the analysis, the specimen had lost 67.5% of its strength, down to only 1,000 kN. This outcome was a consequence of the fact that, in the model, all strips and HBEs at each floor contributed to the degradation, compared to only the first floor elements in the actual experiment.

As mentioned previously, the conservative strip model selected from the calibration of the Qu and Bruneau (2008) specimen was based on result of its first strip to deteriorate. In the initial calibration, 15 strips were used to model the first story infill plate

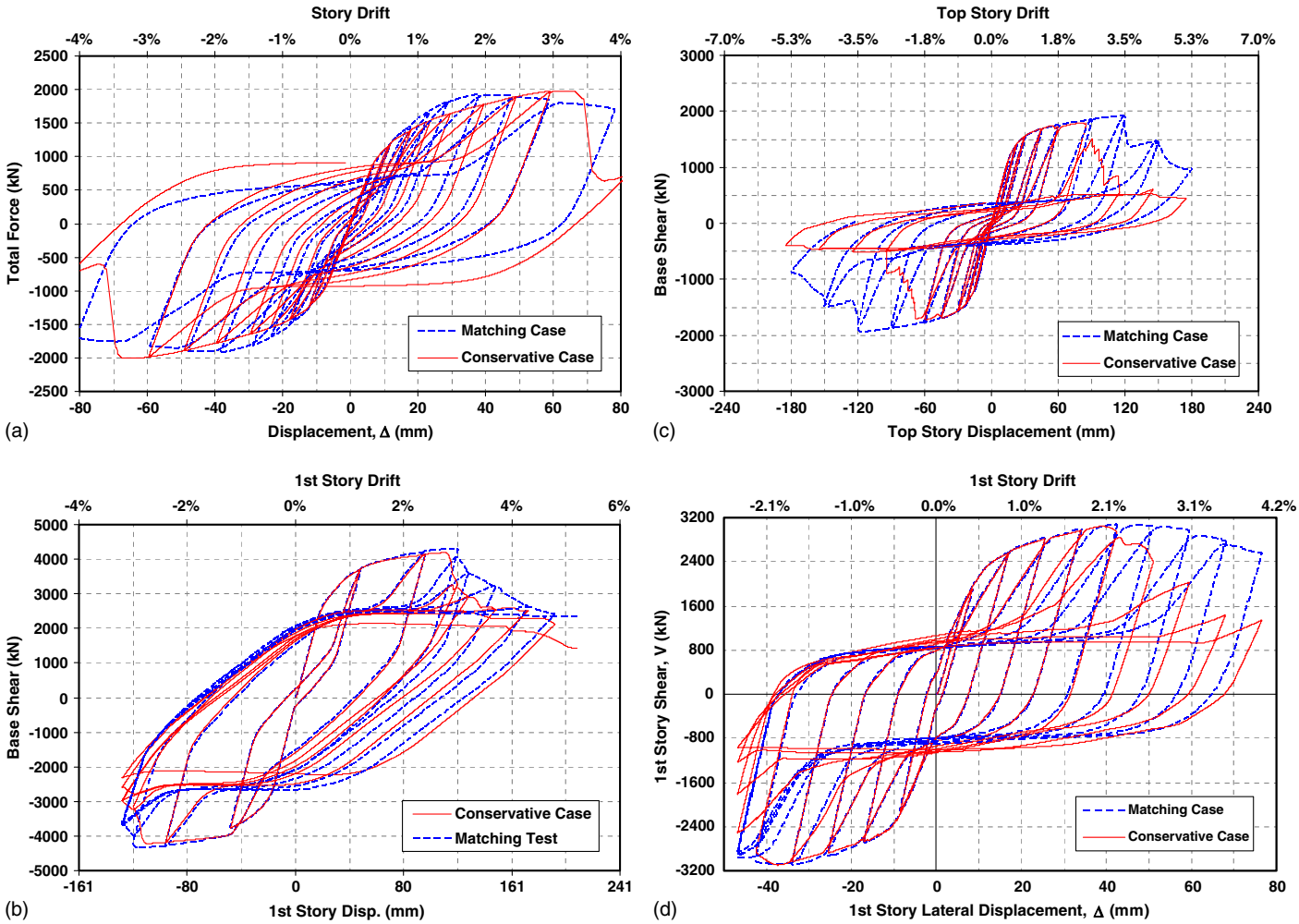

Fig. 7. SPSW specimen hysteresis with the most conservative degradation models applied to calibrated specimens: (a) Vian and Bruneau (2005); (b) Qu and Bruneau (2008); (c) Choi and Park (2009); (d) Driver et al. (1997)

degradation behavior, each with different degradation parameters (i.e., deformation capacities at the capping and failure points) to match the experimental results [Fig. 4(a)]. On average, the deformation capacities of these strips at the capping and failure points were $9\delta_y$ and $10.7\delta_y$, respectively (corresponding to 1.5 and 1.8% axial strain, respectively). When using these average results for the infill plate deterioration models instead of using the result of the first strip to deteriorate, marginal differences were observed in the two-story and three-story SPSW specimens (detailed results are not reported here). Assuming that the marginal differences would also be the case for the other two specimens (i.e., comparable to the results shown in Fig. 7), the average deformation capacities were selected for the final deterioration model for strips, as shown in Fig. 8(a). This was necessary to avoid an overly conservative deterioration model for strips in the general case of SPSWs.

At the time of this writing, no SPSW specimen has been tested up to extreme drifts (i.e., 10% drift). Among the currently available experimental data (Table 1), the maximum drift to which SPSW specimens have been tested is 5.6% drift. For collapse assessment of SPSW using incremental dynamic analysis [as addressed in the companion paper (Purba and Bruneau 2014b)], it is important to investigate specimen behaviors up to such extreme drifts because this may condition the results. For this purpose, another set of analyses was conducted on all calibrated specimens up to 10% drift. The deterioration of boundary elements was modeled to linearly decrease to zero strength when cross-sectional rotation reached 0.103 rad. At the fiber level, this corresponds to 0.057 strains in the farthest fiber from the neutral axis.

During the first analysis of the Qu and Bruneau (2008) specimen subjected to such an extreme drift, a numerical convergence problem developed after the specimen experienced 6% drift. Further investigation revealed that the primary source of the problem was the inability of the boundary elements modeled with fiber elements to sustain axial loads after most of the fibers had lost their flexural strength at large drift. To solve this problem, it an elasto-plastic material was assigned for fibers on the web of boundary elements and a deteriorating material model was assigned for the fibers located on the bottom and top flange of the cross section, as shown in Fig. 8(b). This technique made it possible for the analyses to execute fully when the structures experienced drifts of up to 10%. In other words, this approach was equivalent to having the fibers on the web of a cross section reserved to sustain axial loads when all other fibers had lost their capacity owing to significantly large cross-sectional rotations. As a consequence of this approach, boundary elements actually exhibit residual flexural strength when reaching 0.103 rad, as opposed to the zero strength originally intended. However, for W-sections commonly used in North America, the web of W-shapes contributes, on average, approximately up to 20% of the total plastic moment of a section. Therefore, the preceding approach was deemed acceptable, particularly

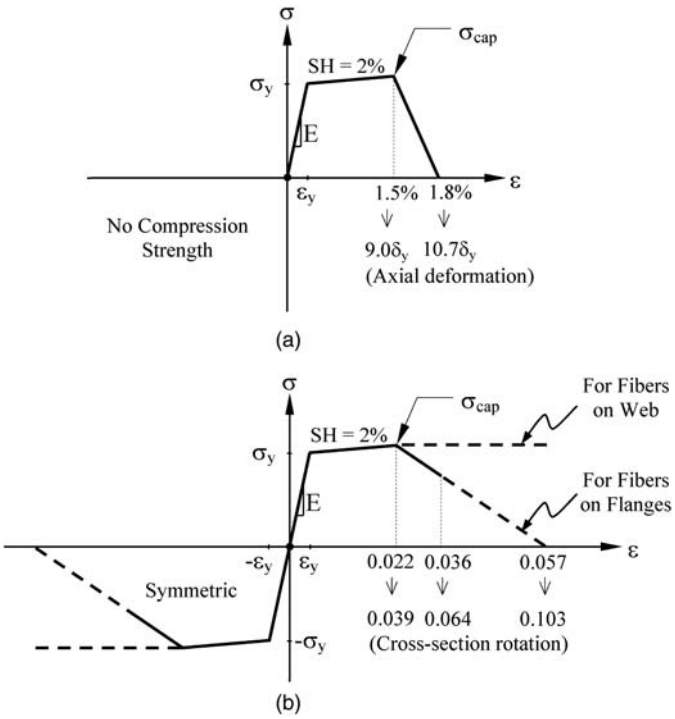

Fig. 8. Final degradation models: (a) strips; (b) boundary elements

considering that during incremental dynamic analysis, gravity leaning columns cause global structural collapse once a structure undergoes significant lateral displacements at relatively small residual strength. At the end of the 10% drift cycle, all specimens have lost a significant amount of their ability to sustain lateral loads and the remaining residual strengths represent the contribution of the boundary elements (from the bilinear elasto-plastic fibers in their webs).

Conclusions

Deterioration models for infill plates and boundary elements were developed in a format compatible with the FEMA P695 methodology (2009b) for use in the collapse assessment of SPSWs having infill plates designed to sustain different percentages of the applied lateral loads. Based on a review of 36 SPSW specimens, the possible causes of deterioration of structural components that lead to failures of SPSWs were identified: deteriorations associated with WT, flexural or shear FBE, and IBE. Of these deterioration modes, only the first two were considered to quantify the deterioration parameters of SPSWs, because the last two modes can be prevented by designing boundary elements according to capacity design principles and selecting seismically compact sections. The parameters for the chosen deteriorated material models for infill plates and boundary elements were statistically quantified and calibrated to four selected SPSW specimens varying from one to four stories.

The final deterioration model for boundary elements was characterized with strain hardening of 2%, up to a capping point at 0.04 rad, and gradually losing its entire strength at 0.10 rad. However, this deterioration material model was only applied to fibers at the bottom and top flanges of W-sections, whereas those on the webs were modeled with no degradation to maintain numerical stability during the analysis by allowing boundary elements to resist axial forces. Regarding the infill plates, strips were modeled to begin deteriorating at 1.5% axial strain (i.e., $9.0\delta_y$) and rather quickly lost their capacity to sustain loads owing to plate tearing, at 1.8% axial strain (i.e., $10.7\delta_y$). All strips were established with the same deterioration model, irrespective of the location of strips (i.e., corner or middle strips or floor level). This model exhibited stable behavior and was found to provide an acceptable match with experimental results for the perspective of investigating seismic performance of SPSW having infill plates designed considering two different design philosophies. Using these deterioration models, the companion paper (Purba and Bruneau 2014b) presents the results of these seismic performance assessments, including the development of SPSW archetypes, the formulation of a nonlinear analytical model, the results of nonlinear static and dynamic analyses (i.e., pushover and incremental dynamic analyses), and the evaluation of collapse performance.

Acknowledgments

This work was supported in part by the George E. Brown, Jr. Network for Earthquake Engineering Simulation (NEES) Program of the National Science Foundation under NSF NEESR Award Number CMMI-0830294. The financial support of the Fulbright Indonesia Presidential Scholarship to the first author is gratefully appreciated. However, any opinions, findings, conclusions, and recommendations presented in this paper are those of the writers and do not necessarily reflect the views of the sponsors.

References

AISC. (2010). "Seismic provisions for structural steel buildings." *ANSI/AISC 341-10*, Chicago.

ASCE. (2013). "Seismic evaluation and retrofit of existing buildings." *ASCE/SEI 41-13*, Reston, VA.

Astaneh-Asl, A., and Zhao, Q. (2002). "Cyclic behavior of steel shear wall systems." *Proc., Annual Stability Conf., Structural Stability Research Council*, American Institute of Steel Construction (AISC), Chicago, IL.

Baldvins, N. M., Berman, J. W., Lowes, L. N., Janes, T. M., and Lowa, N. A. (2012). "Fragility functions for steel plate shear walls." *Earthquake Spectra*, 28(2), 405–426.

Behbahanifard, M. R., Grondin, G. Y., and Elwi, A. E. (2003). "Experimental and numerical investigation of steel plate shear wall." *Structural Engineering Rep. 254*, Dept. of Civil Engineering, Univ. of Alberta, Edmonton, AB, Canada.

Berman, J. W., and Bruneau, M. (2005). "Experimental investigation of light-gauge steel plate shear walls." *J. Struct. Eng.*, 10.1061/(ASCE)0733-9445(2005)131:2(259), 259–267.

Caccese, V., Elgaaly, M., and Chen, R. (1993). "Experimental study of thin steel plate shear walls under cyclic load." *J. Struct. Eng.*, 10.1061/(ASCE)0733-9445(1993)119:2(573), 573–587.

Canadian Standards Association (CSA). (2009). "Design of steel structures." *CAN/CSA S16-09*, Willowdale, ON, Canada.

Choi, I.-R., and Park, H.-G. (2008). "Ductility and energy dissipation capacity of shear-dominated steel plate walls." *J. Struct. Eng.*, 10.1061/(ASCE)0733-9445(2008)134:9(1495), 1495–1507.

Choi, I.-R., and Park, H.-G. (2009). "Steel plate shear walls with various infill plate designs." *J. Struct. Eng.*, 10.1061/(ASCE)0733-9445(2009)135:7(785), 785–796.

Choi, I.-R., and Park, H.-G. (2010). "Hysteresis model of thin infill plate for cyclic nonlinear analysis of steel plate shear walls." *J. Struct. Eng.*, 10.1061/(ASCE)ST.1943-541X.0000244, 1423–1434.

Clayton, P. M., Berman, J. W., and Lowes, L. N. (2012). "Seismic design and performance of self-centering steel plate shear walls." *J. Struct. Eng.*, 10.1061/(ASCE)ST.1943-541X.0000421, 22–30.

Dastfan, M., and Driver, R. G. (2008). "Flexural stiffness limits for frame members of steel plate shear wall systems." *Proc., Annual Stability Conf., Nashville*, Structural Stability Research Council, Rolla, MO.

Dowden, D., and Bruneau, M. (2014). "Analytical and experimental investigation of self-centering steel plate shear walls." *Tech. Rep. MCEER-14-0010*, Multidisciplinary Center for Earthquake Engineering Research, State Univ. of New York at Buffalo, Buffalo, New York.

Driver, R. G., Kulak, G. L., Kennedy, D. J. L., and Elwi, A. E. (1997). "Seismic behavior of steel plate shear walls." *Structural Engineering Rep. 215*, Dept. of Civil Engineering, Univ. of Alberta, Edmonton, AB, Canada.

Elgaaly, M. (1998). "Thin steel plate shear walls behavior and analysis." *Thin Walled Struct.*, 32(1–3), 151–180.

FEMA. (2000). "Prestandard and commentary for seismic rehabilitation of buildings." *FEMA Rep. No. 356*, ASCE for FEMA, Washington, DC.

FEMA. (2009a). "Effects of strength and stiffness degradation on seismic response." *FEMA Rep. No. P440A*, Applied Technology Council for FEMA, Washington, DC.

FEMA. (2009b). "Quantification of building seismic performance factors." *FEMA Rep. No. P695*, Applied Technology Council for FEMA, Washington, DC.

Haselton, C. B., and Deierlein, G. G. (2007). "Assessing seismic collapse safety of modern reinforced concrete frame buildings." *John A. Blume Earthquake Engineering Center, Technical Rep. No. 156*, Stanford Univ., Stanford, CA.

Ibarra, L. F., and Krawinkler, H. (2005). "Global collapse of frame structures under seismic excitations." *John A. Blume Earthquake Engineering Center, Technical Rep. No. 152*, Dept. of Civil Engineering, Stanford Univ., Stanford, CA.

Li, C.-H., Tsai, K.-C., Lin, C.-H., and Chen, P.-C. (2010). "Cyclic tests of four two-story narrow steel plate shear walls. Part 2: Experimental results and design implications." *Earthquake Eng. Struct. Dyn.*, 39(7), 801–826.

Lignos, D. G., and Krawinkler, H. (2009). "Sidesway collapse of deteriorating structural systems under seismic excitations." *John A. Blume Earthquake Engineering Center, Technical Rep. No. 172*, Dept. of Civil Engineering, Stanford Univ., Stanford, CA.

Lubell, A. S., Prion, H. G. L., Ventura, C. E., and Rezai, M. (2000). "Unstiffened steel plate shear wall performance under cyclic loading." *J. Struct. Eng.*, 10.1061/(ASCE)0733-9445(2000)126:4(453), 453–460.

OpenSees version 2.0 [Computer software]. Berkeley, CA, Pacific Earthquake Engineering Research Center, Univ. of California.

Park, H. G., Kwack, J. H., Jeon, S. W., Kim, W. K., and Choi, I. R. (2007). "Framed steel plate wall behavior under cyclic lateral loading." *J. Struct. Eng.*, 10.1061/(ASCE)0733-9445(2007)133:3(378), 378–388.

Purba, R., and Bruneau, M. (2014a). "Seismic performance of steel plate shear walls considering various design approaches." *Tech. Rep. MCEER-14-0005*, Multidisciplinary Center for Earthquake Engineering Research, State Univ. of New York at Buffalo, Buffalo, New York.

Purba, R., and Bruneau, M. (b). "Seismic performance of steel plate shear walls considering two different design philosophies of infill plates. II: Assessment of collapse potential." *J. Struct. Eng.*, 10.1061/(ASCE)ST.1943-541X.0001097, 04014161.

Qu, B., and Bruneau, M. (2008). "Seismic behavior and design of boundary frame members of steel plate shear walls." *Technical Rep. MCEER-08-0012*, Multidisciplinary Center for Earthquake Engineering Research, Buffalo, New York.

Qu, B., and Bruneau, M. (2009). "Design of steel plate shear walls considering boundary frame moment resisting action." *J. Struct. Eng.*, 10.1061/(ASCE)ST.1943-541X.0000069, 1511–1521.

Roberts, T., and Sabouri-Ghomi, S. (1991). "Hysteretic characteristics of unstiffened plate shear panels." *Thin Walled Struct.*, 12(2), 145–162.

Song, J.-K., and Pincheira, J. A. (2000). "Seismic analysis of older reinforced concrete columns." *Earthquake Spectra*, 16(4), 817–851.

Thorburn, L. J., Kulak, G. L., and Montgomery, C. J. (1983). "Analysis of steel plate shear walls." *Structural Engineering Rep. No. 107*, Dept. of Civil Engineering, Univ. of Alberta, Edmonton, AB, Canada.

Vian, D., and Bruneau, M. (2005). "Steel plate shear walls for seismic design and retrofit of building structures." *Tech. Rep. MCEER-05-0010*, Multidisciplinary Center for Earthquake Engineering Research, State Univ. of New York at Buffalo, Buffalo, New York.